Chapter 2
Linear Oscillator and a Non-ideal Energy Source

In the non-ideal oscillator-motor system there is an interaction between the motions of the oscillator and of the motor: the motor has an influence on the oscillator and vice versa the motion of the oscillator affects the motion of the motor. It is in contrary to the ideal system, where only the motor has an influence on the oscillator motion and the influence of the oscillator on the motor is negligible (Kononenko 1969, 1980; Nayfeh and Mook 1979). In this chapter the linear oscillator coupled to a non-ideal energy source is considered. A significant number of researches in dynamics of linear oscillator coupled with the non-ideal energy source is already done (see overviews Balthazar et al. 2003; Cveticanin 2010; References given in these papers and, recently published papers Souza et al. 2005a, b; Dantas and Balthazar 2007; Felix et al. 2009, 2011; Samantaray 2010; Kovriguine 2012; Tusset et al. 2012a, b etc). In the non-ideal system with linear oscillator the connection of the system with the fixed element is with an elastic element with linear property. Usually, a motor is supported on a cantilever beam which has linear properties or a motor is settled on the linear foundation (Dimentberg et al. 1997; Warminski et al. 2001). In the literature the vibration of the system is determined analytically and the result is compared with numerically obtained value. Discussing the results the special attention is given to the phenomenon called 'Sommerfeld effect' which is a property of the non-ideal systems.

The chapter is divided into three sections where three types of oscillator-motor systems are considered: the one degree-of-freedom linear oscillator connected with a non-ideal energy source, oscillator with variable mass excited with anon-ideal source and the oscillator with clearance.

In the Sect. 2.1, a motor supported on a cantilever beam with linear elastic properties is considered. The system is modelled and an analytical solving procedure is developed for obtaining of the approximate solutions. The steady-state motion in the resonant working regime is given and the Sommerfeld effect is explained. An analog mechanical model is introduced for better explanation of the problem

(Goncalves et al. 2014). Conditions for motion stability of the non-ideal system with linear oscillator are determined.

In the Sect. 2.2, the oscillator with variable mass with non-ideal excitation is investigated. The system is described with two coupled equations with time variable parameters. The analytical and numerical solution of the problem is considered. The influence of the parameter variation on the behavior of the system is discussed.

Section 2.3 deals with an oscillator with clearance forced with a non-ideal source. The elastic force in the spring is discontinual and it causes some additional disturbances in the motion of the system. Both, the transient and the steady-state motion of the system are investigated. In this system beside regular motion, chaotic motion is evident (Lin and Ewins 1993). Conditions for chaos are obtained and a method for chaos control is developed (Zukovic and Cveticanin 2009).

2.1 Simple Degree of Freedom Oscillator Coupled with a Non-ideal Energy Source

Let us consider a motor settled on a table where it is supposed that the motor is a non-ideal energy source while the support represents an oscillator. The model of a motor - support system is usually modelled as a cantilever beam with a concentrated mass positioned at its free end (see Fig. 2.1).

The beam is made of steel and its properties are defined by Young's modulus E, density ρ, the length L, the cross-sectional area S and the second moment of area I. The beam bending stiffness is $k = 3EI/L^3$, and its mass is $m_b = \rho SL$. If M_c represents the mass of the electric motor, the total concentrated mass at the end of the beam is $m_1 = M_c + 0.23m_b$ (Goncalves et al. 2014). The motor has moment of inertia J. It is known that the rotor of the motor suffers from unbalance. Rotor is never perfectly balanced and the unbalance mass is $m_2 = m_b$ that rotates at a distance d from the motor shaft center. For low amplitudes of oscillation when the higher order modes are neglected, it is possible to write an expression for the first bending natural frequency ω_0 of the beam with concentrated mass as

$$\omega_0 = \sqrt{\frac{3EI}{L^3(m_1 + m_2)}}. \tag{2.1}$$

Fig. 2.1 Cantilever beam with a concentrated mass and an unbalanced motor
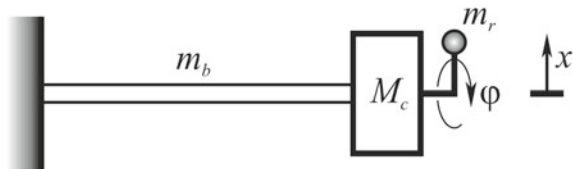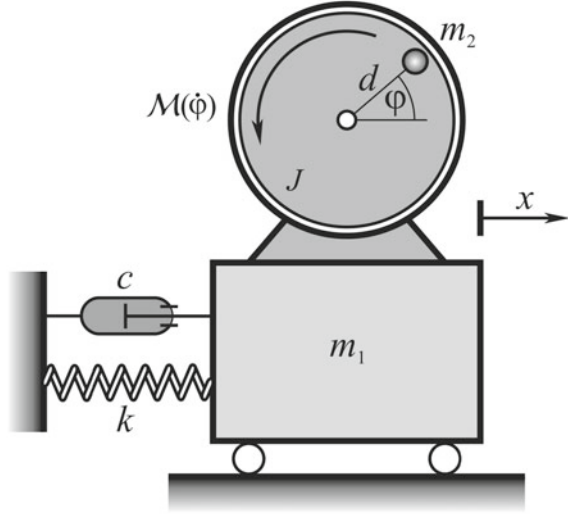
Fig. 2.2 Model of a
spring-mass-damper
oscillator and a motor with
unbalanced mass

Due to rigidity and damping properties of the beam, it can be modified as a spring-mass-damper oscillator. Then, the cantilever beam - motor system is represented as a cart with mass m_1, connected with a spring and damper to the fixed plane, and coupled with unbalanced mass (Fig. 2.2).

The system has two degrees of freedom. The cart displacement is defined by x and the motor angular position is represented by φ. The kinetic energy of the system T is

$$T = \frac{m_1}{2}\dot{x}^2 + \frac{J}{2}\dot{\varphi}^2 + \frac{m_2}{2}v_2^2, \tag{2.2}$$

where v_2 is the velocity of the unbalance mass. For position coordinates of the motor unbalanced mass m_2: $x_2 = x + d\cos\varphi$ and $y_2 = d\sin\varphi$, the velocity follows as

$$v_2 = \sqrt{\dot{x}_2^2 + \dot{y}_2^2} = \sqrt{\dot{x}^2 + d^2\dot{\varphi}^2 - 2d\dot{x}\dot{\varphi}\sin\varphi}. \tag{2.3}$$

Substituting (2.3) into (2.2) we obtain

$$T = \frac{1}{2}(m_1 + m_2)\dot{x}^2 + \frac{1}{2}(J + m_2d^2)\dot{\varphi}^2 - m_2d\dot{x}\dot{\varphi}\sin\varphi. \tag{2.4}$$

If the gravity potential energy is neglected, the systems potential energy is

$$U = \frac{1}{2}kx^2. \tag{2.5}$$

Equations of motion of the system are obtained by using the Lagrange's differential equations of motion

$$
\begin{aligned}
\frac{d}{dt}\frac{\partial T}{\partial \dot{x}} - \frac{\partial T}{\partial x} + \frac{\partial U}{\partial x} &= Q_x, \\
\frac{d}{dt}\frac{\partial T}{\partial \dot{\varphi}} - \frac{\partial T}{\partial \varphi} + \frac{\partial U}{\partial \varphi} &= Q_\varphi,
\end{aligned}
\tag{2.6}
$$

where Q_x and Q_φ are generalized forces. The non-conservative force in x direction is the damping force $Q_x = -c\dot{x}$ with the damping coefficient c, while the generalized force Q_φ corresponds to the torque $\mathcal{M}(\dot{\varphi})$ applied to motor.

Using relations (2.4)–(2.6) and the generalized force, the cart equation of motion is

$$
(m_1 + m_2)\,\ddot{x} + c\dot{x} + kx = m_2 d\left(\ddot{\varphi}\sin\varphi + \dot{\varphi}^2\cos\varphi\right),
\tag{2.7}
$$

and the motion of the motor shaft is given by

$$
\left(J + m_2 d^2\right)\ddot{\varphi} = m_2 d\ddot{x}\sin\varphi + \mathcal{M}(\dot{\varphi}).
\tag{2.8}
$$

Equations (2.7) and (2.8) are autonomous and nonlinear.

2.1.1 Analytical Solving Procedure

Let us introduce the dimensionless length and time variables

$$
y = \frac{x}{d},
\tag{2.9}
$$

$$
\tau = \omega t,
\tag{2.10}
$$

and parameters

$$
\begin{aligned}
\varepsilon\zeta_1 &= \frac{c}{\sqrt{k(m_1 + m_2)}}, \quad \varepsilon = \frac{m_2 d}{X(m_1 + m_2)}, \\
\varepsilon\eta_1 &= \frac{m_2 dX}{J + m_2 d^2}, \quad \mathcal{M}(\varphi') = \frac{\mathcal{M}(\dot{\varphi})}{\omega^2\left(J + m_2 d^2\right)}.
\end{aligned}
\tag{2.11}
$$

Dimensionless differential equations of motion of the oscillatory system follow as

$$
\begin{aligned}
y'' + y &= -2\varepsilon\zeta_1 y' + \varepsilon\left(\varphi''\sin\varphi + \varphi'^2\cos\varphi\right), \\
\varphi'' &= \varepsilon\eta_1 y''\sin\varphi + \varepsilon\,\mathcal{M}(\varphi'),
\end{aligned}
\tag{2.12}
$$

where

$$\omega = \sqrt{\frac{k}{m_1 + m_2}}, \tag{2.13}$$

is the frequency of the system, $(') \equiv d/d\tau$ and X is the length characteristic of the amplitude of the motion of the motor Nayfeh and Mook (1979). Assuming that the parameter ε is small, Eq. (2.12) are with small nonlinear terms. For computational reasons it is convenient to rewrite (2.12) into a system of first order equations. Accordingly, we let

$$y = a\cos(\varphi + \psi), \tag{2.14}$$

where a, φ and ψ are functions of τ. Generally, it cannot be expected that the frequency of the rectilinear motion $(\varphi' + \psi')$ to be the same as the angular speed of the rotor φ'. Hence, ψ is included in the argument.

We are considering the motion near resonance and it is convenient to introduce a detuning parameter Δ as follows

$$\varphi' = 1 + \Delta. \tag{2.15}$$

Hence ψ is used to distinguish between the speed of the rotor and the actual frequency of the rectilinear motion, while Δ is used to distinguish between the speed of the rotor and the natural frequency of the rectilinear motion.

Using the method of variation of parameters, we put

$$a'\cos(\varphi + \psi) - a(\Delta + \psi')\sin(\varphi + \psi) = 0, \tag{2.16}$$

so that

$$y' = -a\sin(\varphi + \psi), \tag{2.17}$$

and

$$y'' = -a'\sin(\varphi + \psi) - a(1 + \Delta + \psi')\cos(\varphi + \psi). \tag{2.18}$$

Substituting (2.15), (2.17) and (2.18) into (2.12) leads to

$$-a'\sin(\varphi + \psi) - a(\Delta + \psi')\cos(\varphi + \psi) \tag{2.19}$$
$$= \varepsilon\Delta'\sin\varphi + \varepsilon(1 + \Delta)^2\cos\varphi + 2\varepsilon\zeta_1 a\sin(\varphi + \psi),$$

and

$$\Delta' = -\varepsilon\eta_1\left(a'\sin(\varphi + \psi) + \varepsilon a(1 + \Delta + \psi')\cos(\varphi + \psi)\right)\sin\varphi + \varepsilon\mathcal{M} \tag{2.20}$$

where $\mathcal{M} = \mathcal{M}\left(\varphi'\right)$. Solving (2.16) and (2.19) for a' and ψ' produces

$$a' = \varepsilon\Delta'\sin\varphi - \varepsilon(1+\Delta)^2\cos\varphi - 2\varepsilon\zeta_1 a\sin(\varphi+\psi)\sin(\varphi+\psi), \qquad (2.21)$$

$$\psi' = -\Delta - \frac{\varepsilon}{a}\Delta'\sin\varphi - \frac{\varepsilon}{a}(1+\Delta)^2\cos\varphi - 2\varepsilon\zeta_1\sin(\varphi+\psi)\cos(\varphi+\psi). \qquad (2.22)$$

Equations (2.20)–(2.22) are equivalent to the system (2.12). No approximations have been made yet. These equations show that Δ' and a' are $O(\varepsilon)$. We restrict our attention to a narrow band of frequencies around the natural frequency

$$\Delta = \varepsilon\sigma. \qquad (2.23)$$

Δ and Δ' are $O(\varepsilon)$, and it follows from (2.22) that ψ' is also $O(\varepsilon)$. As a first simplification we neglect all terms $O(\varepsilon^2)$ appearing in (2.20)–(2.22) and we obtain

$$\Delta' = \varepsilon\left(\mathcal{M} - \eta_1 a\cos(\varphi+\psi)\sin\varphi\right), \qquad (2.24)$$

$$a' = -\varepsilon\left(\cos\varphi + 2\zeta_1 a\sin(\varphi+\psi)\right)\sin(\varphi+\psi), \qquad (2.25)$$

$$\psi' = -\Delta - \frac{\varepsilon}{a}\left(\cos\varphi + 2\zeta_1\sin(\varphi+\psi)\right)\cos(\varphi+\psi). \qquad (2.26)$$

To solve the Eqs. (2.24)–(2.26) in exact analytical form is not an easy task. The approximate solution is obtained by applying of the averaging procedure. We consider a, σ and ψ to be constant over one cycle and average the equations over one cycle. The result is

$$\Delta' = \varepsilon\left(\mathcal{M} + \frac{1}{2}\eta_1 a\sin\psi\right), \qquad (2.27)$$

$$a' = -\varepsilon\left(\frac{1}{2}\sin\psi + a\zeta_1\right), \qquad (2.28)$$

$$\psi' = -\varepsilon\left(\sigma + \frac{1}{2a}\cos\psi\right). \qquad (2.29)$$

At this point, let us mention the difference between ideal and non-ideal systems. For the ideal system relation (2.27) is not a governing equation as σ is specified and (2.28) and (2.29) are solved for a and ψ. For the non-ideal system the Eqs. (2.27)–(2.29) are solved for a, Δ and ψ with $\mathcal{M}$ as a control setting.

2.1.2   Steady-State Solution and Sommerfeld Effect

For steady-state responses, a', Δ' and ψ' are zero, i.e., Eqs. (2.27)–(2.29) transform into

$$\mathcal{M} + \frac{1}{2}\eta_1 a \sin \psi = 0, \tag{2.30}$$

$$\frac{1}{2} \sin \psi + a\zeta_1 = 0, \tag{2.31}$$

$$\sigma + \frac{1}{2a} \cos \psi = 0. \tag{2.32}$$

Combining (2.31) and (2.32) yields

$$a = \frac{1}{2\sqrt{\zeta_1^2 + \sigma^2}}, \tag{2.33}$$

while combining (2.30) and (2.31) gives

$$\mathcal{M} = \eta_1 \zeta_1 a^2. \tag{2.34}$$

The phase is given by

$$\psi = \cos^{-1}(-2a\sigma) = \sin^{-1}(-2a\zeta_1). \tag{2.35}$$

Recalling the definitions of the dimensionless variables, we rewrite these results in terms of the original physical variables as

$$Xa = \frac{\omega m_2 d}{\sqrt{c^2 + 4(\omega - \dot{\varphi})^2(m_1 + m_2)^2}}, \tag{2.36}$$

$$\psi = \tan^{-1}\left(-\frac{2(m_1 + m_2)(\omega - \dot{\varphi})}{c}\right), \tag{2.37}$$

and

$$\mathcal{M}(\dot{\varphi}) = \frac{c\omega k m_2 d X}{2\left(c^2 + 4(\omega - \dot{\varphi})^2(m_1 + m_2)^2\right)}, \tag{2.38}$$

where (Xa) is the physical amplitude of the motion and according to (2.35), $-\pi/2 < \psi < 0$. The solving procedure is as it follows: first, the (2.38) is solved for $\dot{\varphi}$ and then, the amplitude and phase from (2.36) and (2.37) are obtained.

To solve the Eq. (2.38) it is necessary to know the torque function of the motor. Namely, the torque of the motor contains two terms: the characteristic of the motor $L(\dot{\varphi})$ and the resisting moment $H(\dot{\varphi})$ due primarily to windage of the rotating parts outside the motor

$$\mathcal{M}(\dot{\varphi}) = L(\dot{\varphi}) - H(\dot{\varphi}).$$

Generally, $L(\dot{\varphi})$ and $H(\dot{\varphi})$ are determined experimentally. Various types of mathematical description of the motor property are suggested. One of the most often applied and the simplest one is the linear mode which is a function of the angular velocity $\dot{\varphi}$

$$\mathcal{M}(\dot{\varphi}) = M_0 \left(1 - \frac{\dot{\varphi}}{\Omega_0}\right), \tag{2.39}$$

and depends on two constant parameters M_0 and Ω_0 which define the limited source of power as the angular velocity increases. The expression (2.39) defines the characteristic curve of the motor shown in Fig. 2.3, where for angular velocities greater than Ω_0 the torque reduces to zero and when the angular velocity is zero the torque is maximum. Figure 2.3 is an illustrative example in which Eq. (2.39) is valid for positive values of torque and angular velocity.

In this section the calculation is done for the linear torque function (2.39). Solving (2.36)–(2.38) with (2.39) the frequency - response relation is obtained. In Fig. 2.4 the corresponding diagram is plotted. For the ideal linear system the frequency-response diagram is a continual curve presented with a solid line in Fig. 2.4. For the non-ideal system the curves are obtained by allowing the system to achieve a steady-state motion while the control was fixed. Then the amplitude of the steady-state response was calculated. The control was then changed very slightly and held in the new position until a new steady state was achieved. For increasing of angular frequency the amplitude increases up to T and jumps to H and moves in right-hand side direction along the amplitude curve. For the decreasing frequency the amplitude increases up to R and suddenly jumps to P and decreases continually along the solid line curve. We note that there are gaps where no steady-state response exists. The gaps are not the same in the two directions but there is some overlap. The arrows indicate the change brought about by slowly increasing or decreasing the control setting in a

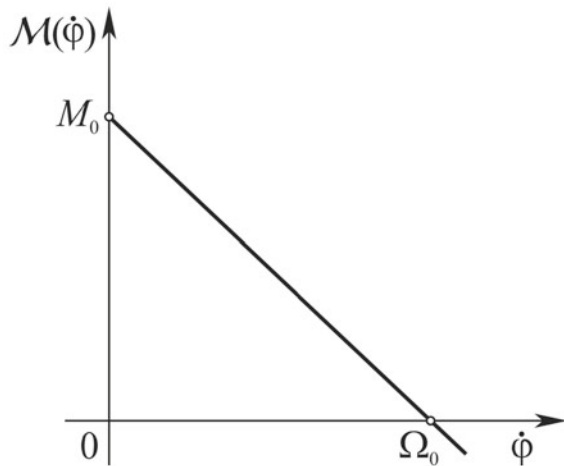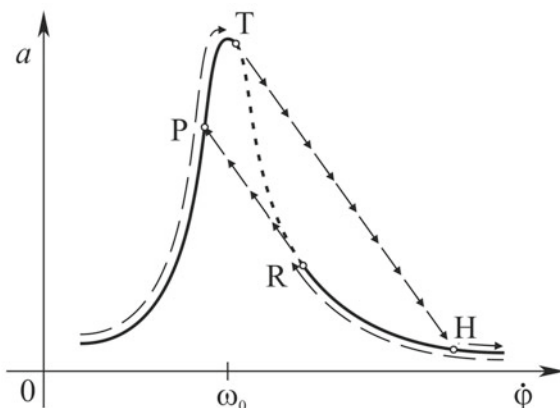**Fig. 2.3** Motor torque characteristic curve

Fig. 2.4 Frequency-response curves for ideal system (– – – –) and non-ideal system (→→) (Nayfeh and Mook 1979)

non-ideal system. We note that the non-ideal system cannot be made to respond at a frequency between T and H by simply increasing the control setting form a low value. In contrast, the ideal system can respond also at frequencies between T and H. When the control setting is continually decreased, the system cannot be made to respond between R and P. In other words, the right side of the resonance spike between T and R cannot be reached by either continually increasing or continually decreasing the control setting. Though the system is linear, the non-ideal source causes a jump phenomenon to occur.

At the left-hand side of the frequency-response curve the input power is relatively low. As the input power increases, the amplitude of the response increases noticeably while the frequency changes only slightly, especially along the portion of the curve between P and T. Here a relatively large increase in power causes a relatively large increase in the amplitude and practically no change in the frequency.

At T the character of the motion suddenly changes. An increase in the input power causes the amplitude to decrease and the frequency to increase considerably. This phenomenon is called Sommerfeld effect. It was discovered by Arnold Sommerfeld in 1902, commented in a book of Kononenko (1969) and described in the book of Nayfeh and Mook (1976). The jump phenomena in the amplitude-frequency curve for the non-ideal system is remarked during passage through resonance. In this working regime special properties of the non-ideal source are caused. Namely, in the region before resonance as the power supplied to the source increases, the RPM of the energy source (motor) increases accordingly. But, the closed motor speed moves toward the resonance frequency the more power the source requires to increase the motor speed. Near resonance it appears that additional power supplied to the motor will only increase the amplitude of the response with little effect on the RPM of the motor, and the amplitude of vibration increases. In non-ideal vibrating systems the passage through resonance requires more input power than is available. As a consequence the vibrating system cannot pass through resonance or requires an intensive interaction between the vibrating system and the energy source to be able

to do it. Strong interaction leads to fluctuating motor speed and fairly large vibration amplitudes appear. The motor may not have enough power to reach higher regimes with low energy consumption as most of its energy is applied to move the structure and not to accelerate the shaft. In fact, the vibrating response provides a certain energy sink.

2.1.3   Model Analogy and Numerical Simulation

To explain the motion in non-ideal system a model analogy is introduced. Let us consider the Eq. (2.38). Substituting (2.39) into (2.8) it is

$$\left(J + m_2 d^2 \right) \ddot{\varphi} = m_2 d \ddot{x} \sin \varphi + M_0 \left(1 - \frac{\dot{\varphi}}{\Omega_0} \right). \qquad (2.40)$$

Discussion of (2.40) follows.

Let us consider a motor mounted on a rigid base. Motion of the cart is eliminated ($\ddot{x} = 0$) and according to (2.40) the mathematical model is

$$\left(J + m_2 d^2 \right) \ddot{\varphi} = M_0 \left(1 - \frac{\dot{\varphi}}{\Omega_0} \right). \qquad (2.41)$$

The physical model which corresponds to (2.41) is a wheel climbing on a ramp. The slope of the ramp is related to the motor inertia defining the rate of the angular velocity.

For a motor with no resistive torque when $\mathcal{M} = M_0$, the angular acceleration is constant and therefore, the angular velocity of the wheel increases by a constant rate (see Fig. 2.5a). The motor torque should be switched off as the desired angular velocity Ω_0 is achieved.

When considering the motor with resistive torque, the angular acceleration is no longer constant and decreases as the angular velocity increases. The system shown in
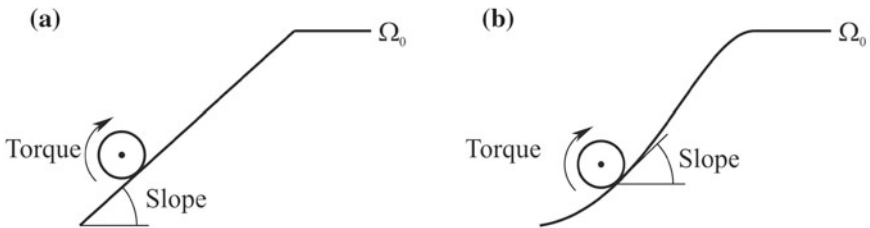

Fig. 2.5 Analogy by a wheel climbing a ramp: **a** a motor with no resistive torque, **b** a motor with resistive torque (Goncalves et al. 2014)

Fig. 2.5b is used to represent the motor with resistive torque where it is more difficult to reach the energy level Ω_0. The rate of velocity changing is no longer linear.

When the motor is mounted on a flexible base, its motion is described with Eq. (2.40). It is clear that the angular acceleration is also a function of the cart motion x. Besides, the motion of the cart is a function of the acceleration and angular velocity of the motor (2.7). In Fig. 2.6 a system which is analog with the motor mounted on a flexible base is represented. Similar to Fig. 2.5a, wheel must climb a ramp to reach the level of energy defined by Ω_0. In this case the ramp path is modified by the cart resonance frequency ω_0.

The resonance frequency is represented by the valley in the ramp path. The deep and the width of the valley in the ramp are related to the amplitude of the motion of the cart and in some cases the wheel can get stuck inside the valley in the ramp path. Numerical simulation is done for frequencies around the cart resonance frequency ω_0. Figure 2.7 shows that when Ω_0 is slightly bigger than ω_0 the angular velocity does not increase. Setting $\Omega_0 = 1.1\omega_0$ the motor does not reach the angular velocity $1.1\omega_0$, instead it will oscillate with angular velocity ω_0. As a consequence, the additional energy increases the amplitude of the displacement of the cart.

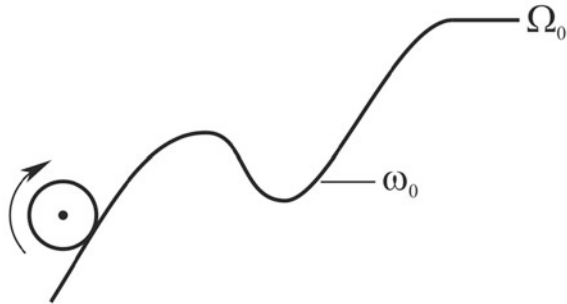**Fig. 2.6** Analogy of the resonance frequency in the ramp path (Goncalves et al. 2014)

Fig. 2.7 The angular velocity as a function of motor constant Ω_0 (Goncalves et al. 2014)
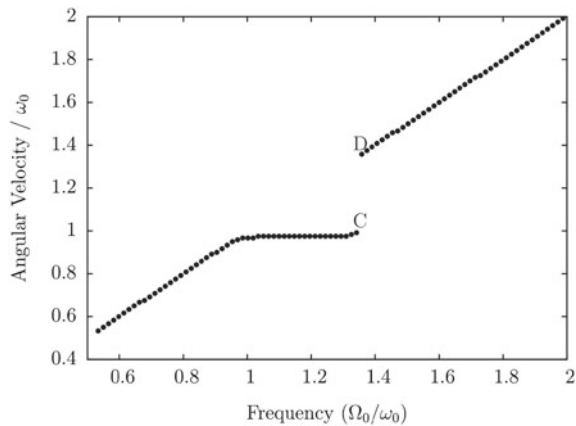
Fig. 2.8 Root mean square
acceleration as a function of
the motor constant Ω_0
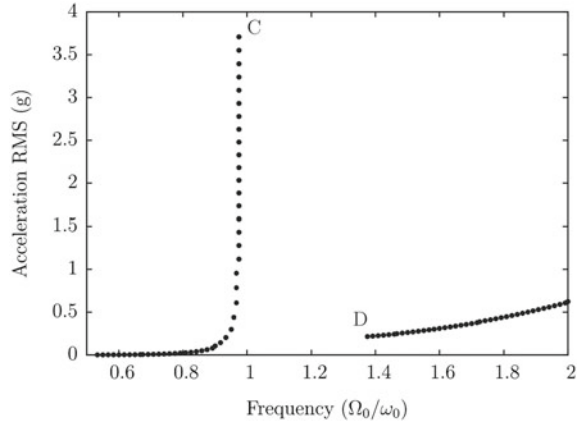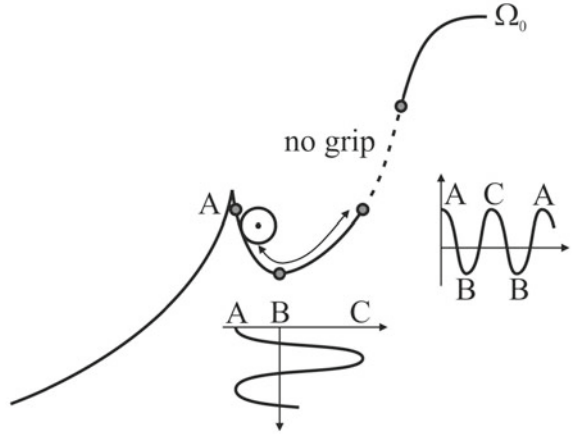(Goncalves et al. 2014)

Fig. 2.9 The analogy of a
wheel climbing a ramp with
the influence of a resonance
frequency (Goncalves et al.
2014)

In Fig. 2.8 the cart root mean square (RMS) magnitude of the acceleration as a
function of the oscillation frequency rate Ω_0/ω_0 is plotted. Based on plots in Figs. 2.7
and 2.8 it is noted that there is a region between C and D without data points. This
region corresponds to a jump phenomenon described by Sommerfeld. The wheel
climbing a ramp is used to explain the jump using the sketch in Fig. 2.9.

The system passing through resonance frequency is represented by the wheel
inside the valley and oscillating between points ABC. There is a region in the ramp
path between points C and D where the wheel does not have grip. The system cannot
stay in energy levels in the region as it will fall in the valley. The width and the
depth of the valley ABC are controlled by the resonance amplitude. The higher the
damping, the shallower the valley.

2.1.4 Stability Analysis

For a given setting of control there can be one, two or three steady state solutions (see Fig. 2.4). To determine which of these steady-state solutions actually corresponds to a realizable motion, we need to consider the stability of motion. Namely, we determine the stability of the steady-state solutions by determining the nature of the singular points which are the solutions of (2.27)–(2.29). To accomplish this, we let

$$a = a_S + a_1, \quad \psi = \psi_S + \psi_1, \quad \Delta = \Delta_S + \Delta_1. \tag{2.42a}$$

Substituting (2.42a) into (2.27)–(2.29) and neglecting all but the linear terms in a_1, ψ_1 and Δ_1, we obtain

$$\Delta_1' = \varepsilon \left(\frac{d\mathcal{M}}{d\varphi'} \varphi_S' \Delta_1 + \frac{1}{2} \eta_1 a_1 \sin(\psi_S) + \frac{1}{2} \eta_1 a_S \psi_1 \cos(\psi_S) \right),$$

$$a_1' = -\varepsilon \left(\frac{1}{2} \psi_1 \cos(\psi_S) + a_1 \alpha_1 \right),$$

$$\psi_1' = -\varepsilon \left(\sigma_1 + \frac{1}{2} \left(\frac{a_1}{a_S^2} \right) \cos(\psi_S) - \frac{1}{2a_S} \psi_1 \sin(\psi_S) \right), \tag{2.43}$$

where $\varepsilon \sigma_1 = \Delta_1$. Linear equation (2.43) have a solution in the form

$$(a_1, \psi_1, \Delta_1) = (a_{10}, \psi_{10}, \Delta_{10}) \exp(\lambda t),$$

i.e.,

$$a_1 = a_{10} \exp(\lambda t), \quad \psi_1 = \psi_{10} \exp(\lambda t), \quad \Delta_1 = \Delta_{10} \exp(\lambda t), \tag{2.44}$$

where λ is the eigenvalue coefficient matrix and $a_{10}, \psi_{10}, \Delta_{10}$ are constants. Substituting (2.44) into (2.43) the characteristic determinant is obtained as

$$\begin{vmatrix} \varepsilon \varphi_S' (\frac{d\mathcal{M}}{d\varphi'})_{\varphi_S'} - \lambda & \frac{\varepsilon}{2} \eta_1 \sin(\psi_S) & \frac{\varepsilon}{2} \eta_1 a_S \cos(\psi_S) \\ 0 & \lambda + \varepsilon \alpha_1 & \frac{1}{2} \varepsilon \cos(\psi_S) \\ 1 & \frac{\varepsilon}{2a_S^2} \cos(\psi_S) & \lambda - \frac{\varepsilon}{2a_S} \sin(\psi_S) \end{vmatrix} = 0,$$

and the characteristic equation is a cubic one

$$0 = \lambda^3 + \lambda^2 \left[\varepsilon \alpha_1 - \frac{\varepsilon}{2a_S} \sin(\psi_S) - \varepsilon \varphi_S' \left(\frac{d\mathcal{M}}{d\varphi'} \right)_{\varphi_S'} \right]$$

$$-\lambda \left[\frac{\varepsilon^2 \alpha_1}{2a_S} \sin(\psi_S) + \frac{\varepsilon^2}{4a_S^2} \cos^2(\psi_S) + \left(\varepsilon \alpha_1 - \frac{\varepsilon}{2a_S} \sin(\psi_S) \right) \varepsilon \varphi_S' \left(\frac{d\mathcal{M}}{d\varphi'} \right)_{\varphi_S'} \right.$$

$$\left. -\frac{\varepsilon}{2} \eta_1 a_S \cos(\psi_S) \right]$$

$$+ \left(\varepsilon \varphi_S' \left(\frac{d\mathcal{M}}{d\varphi'} \right)_{\varphi_S'} \left[\frac{\varepsilon^2 \alpha_1}{2a_S} \sin(\psi_S) + \frac{\varepsilon^2}{4a_S^2} \cos^2(\psi_S) \right] \right.$$

$$+ \frac{\varepsilon^2}{2} \eta_1 \alpha_1 a_S \cos(\psi_S) - \frac{\varepsilon^2}{8} \eta_1 \sin(2\psi_S). \tag{2.45}$$

The solutions are stable and hence the corresponding motions realizable, if the real part of each eigenvalue is negative or zero. Without solving the Eq. (2.45) and using the Routh–Hurwitz principle we can determine the conditions for the stable solution up to the small value $O(\varepsilon^2)$

$$\left[\alpha_1 - \varphi_S' \left(\frac{d\mathcal{M}}{d\varphi'} \right)_{\varphi_S'} \right] a_S \sin(\psi_S) - \frac{1}{4} \sin(2\psi_S) - \varphi_0' \left(\frac{d\mathcal{M}}{d\varphi'} \right)_{\varphi_S'} \eta_1 a_S^3 \cos(\psi_S) > 0. \tag{2.46}$$

Analyzing the relation (2.46) it turns out that the solutions between T and R are unstable, while all those outside this region are stable (Fig. 2.4). As (2.43)$_1$ indicates the parameter, that gives the influence of the motor on the stability, is the slope of the characteristic.

2.2 Oscillator with Variable Mass Excited with Non-ideal Source

There is a significant number of equipment and machines which can be modelled as one degree-of-freedom oscillators with time variable mass. Let us mention some of them: centrifuges, sieves, pumps, transportation devices, etc. For all of them it is common that their mass is varying slowly during the time. The mass variation is assumed to be continual. The excitation of the motion of the equipment is ideal (the excitation force is a harmonic function and the influence of the oscillator on the source is negligible) or non-ideal, where not only the energy source has an influence on the oscillator, but vice versa. In this chapter the oscillator with non-ideal excitation is considered. First the model of the one-degree-of-freedom oscillator with non-ideal excitation is formed. It is a system of two coupled differential equations with time variable parameters. Vibrations close to the resonant regime are considered. For the case when the mass variation is slow the amplitude and frequency of vibration are determined. The Sommerfeld effect for the system where the parameters depend

on the slow time is discussed. Analytical solutions are compared with numerically obtained ones.

2.2.1 Model of the System with Variable Mass

In Fig. 2.10 the model of an oscillator with time variable mass m_1 connected with a motor which is a non-ideal energy source is plotted. The motor is settled on a cart whose mass m_1 is varying in time due to leaking of the contain with velocity u. It is supposed that the mass variation is slow in time. The connection of the oscillating cart to the fixed element has the rigidity k and damping c.
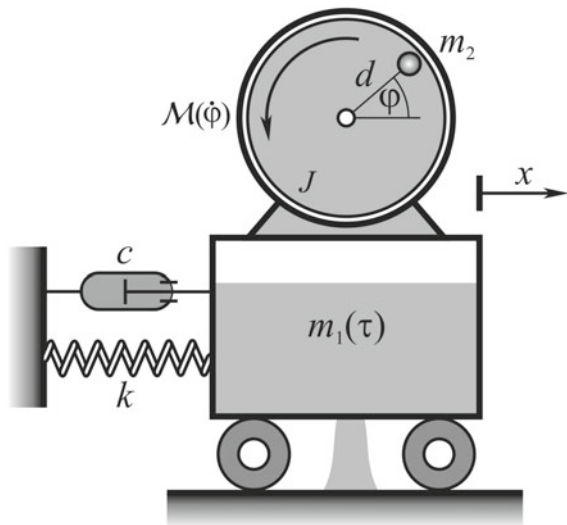
The motor has the moment of inertia J, unbalance m_2 and eccentricity d. The excitation torque of the motor, $\mathcal{M}(\dot{\varphi})$, is the function of the angular velocity $\dot{\varphi}$

$$\mathcal{M}(\dot{\varphi}) = M_0 \left(1 - \frac{\dot{\varphi}}{\Omega_0} \right), \tag{2.47a}$$

where Ω_0 is the steady-state angular velocity. This mathematical model corresponds to asynchronous AC motor (Dimentberg et al. 1997).

To describe the motion of the system, let us assume the two generalized coordinates: the displacement of the oscillator x and the rotation angle of the motor φ. Variation of the mass of the oscillator is assumed to be slow and to be the function of the slow time $\tau = \varepsilon t$, where $\varepsilon << 1$ is a small constant parameter. Equations of motion of the system with time variable mass is in general (Cveticanin 2015)

Fig. 2.10 Model of the non-ideal mass variable system

$$\frac{d}{dt}\frac{\partial T}{\partial \dot{x}} - \frac{\partial T}{\partial x} + \frac{\partial U}{\partial x} = Q_x + Q_R,$$

$$\frac{d}{dt}\frac{\partial T}{\partial \dot{\varphi}} - \frac{\partial T}{\partial \varphi} + \frac{\partial U}{\partial \varphi} = Q_\varphi, \qquad (2.48)$$

where Q_x and Q_φ are generalized forces and Q_R is the generalized reactive force caused by mass variation. If the mass is added or separated with the absolute velocity u in x direction, the generalized reactive force is the product of the velocity u and mass variation dm_1/dt, i.e.

$$Q_R = \frac{dm_1}{dt}u. \qquad (2.49)$$

The non-conservative force in x direction is the damping force $Q_x = -c\dot{x}$ with the damping coefficient c, while the generalized force Q_φ corresponds to the torque $\mathcal{M}(\dot{\varphi})$ applied to motor. The kinetic energy of the system is according to (2.4)

$$T = \frac{1}{2}[m_1(\tau) + m_2]\dot{x}^2 + \frac{1}{2}(J + m_2d^2)\dot{\varphi}^2 - m_2 d\dot{x}\dot{\varphi}\sin\varphi. \qquad (2.50)$$

and the potential energy of the system is according to (2.5)

$$U = \frac{kx^2}{2}. \qquad (2.51)$$

Using (2.50) and (2.51) and also (2.49) equations of motion are due to (2.48)

$$[m_1(\tau) + m_2]\ddot{x} + c\dot{x} + kx = \frac{dm_1(\tau)}{dt}(u - \dot{x}) + m_2 d\left(\ddot{\varphi}\sin\varphi + \dot{\varphi}^2\cos\varphi\right), \quad (2.52)$$

$$\left(J + m_2 d^2\right)\ddot{\varphi} = m_2 d\ddot{x}\sin\varphi + \mathcal{M}(\dot{\varphi}). \qquad (2.53)$$

Assuming that the velocity u is zero, the Eqs. (2.52) and (2.53) transform into

$$[m_1(\tau) + m_2]\ddot{x} + c\dot{x} + kx = -\frac{dm_1(\tau)}{dt}\dot{x} + m_2 d\left(\ddot{\varphi}\sin\varphi + \dot{\varphi}^2\cos\varphi\right), \quad (2.54)$$

$$\left(J + m_2 d^2\right)\ddot{\varphi} = m_2 d\ddot{x}\sin\varphi + \mathcal{M}(\dot{\varphi}). \qquad (2.55)$$

Let us rewrite (2.52) and (2.53) into

$$\ddot{x} + \omega^2(\tau)x = -\varepsilon\zeta(\tau)\dot{x} - \frac{\varepsilon}{m_1(\tau) + m_2}\frac{dm_1(\tau)}{d\tau}\dot{x} \qquad (2.56)$$
$$+ \varepsilon\mu(\tau)\left(\ddot{\varphi}\sin\varphi + \dot{\varphi}^2\cos\varphi\right),$$

$$\ddot{\varphi} = \varepsilon\eta\ddot{x}\sin\varphi + \varepsilon\gamma\mathcal{M}(\dot{\varphi}), \qquad (2.57)$$

where

$$\omega^2(\tau) = \frac{k}{m_1(\tau) + m_2}, \quad \varepsilon\zeta(\tau) = \frac{c}{m_1(\tau) + m_2}, \quad \varepsilon\gamma = \frac{1}{J + m_2 d^2}$$

$$\varepsilon\mu(\tau) = \frac{m_2 d}{m_1(\tau) + m_2}, \quad \varepsilon\eta = \frac{m_2 d}{J + m_2 d^2}. \tag{2.58}$$

In the Eqs. (2.56) and (2.57) the right-hand side terms are of the order of small parameter ε. Analyzing the dimensionless parameters (2.58) it is obvious that the dimensionless frequency ω, damping ζ and excitation γ are functions of slow time. Namely, the mass variation affects these values.

2.2.2 Model of the System with Constant Mass

Let us consider the system with constant mass when $m_1 = const$. Then the dimensionless values ω, ζ and γ in (2.58) are also constant. Assuming that the mass of the system is constant and omitting the terms with the second and higher order of the small parameter ε, relations (2.56) and (2.57) simplify into

$$\ddot{x} + \omega^2 x = -\varepsilon\zeta\dot{x} + \varepsilon\mu\dot{\varphi}^2 \cos\varphi, \tag{2.59}$$

$$\ddot{\varphi} = \varepsilon\eta\ddot{x}\sin\varphi + \varepsilon\gamma\mathcal{M}(\dot{\varphi}). \tag{2.60}$$

Solution of (2.59) and (2.60) is

$$x = a\cos(\varphi + \psi), \tag{2.61}$$

with time derivatives

$$\dot{x} = -a\omega\sin(\varphi + \psi). \tag{2.62}$$

and

$$\dot{\varphi} = \Omega, \tag{2.63}$$

where a is the amplitude of vibration, ψ is the phase angle and Ω is the time derivative of the solution φ. Substituting (2.61)–(2.63) and after some modification the Eqs. (2.59) and (2.60) are rewritten into first order differential equations of motion in new variables a, ψ and Ω

$$\dot{a} = -\varepsilon\zeta a\sin^2(\varphi + \psi) - \varepsilon\mu\frac{\Omega^2}{\omega}\sin(\varphi + \psi)\cos\varphi, \tag{2.64}$$

$$\dot{\psi} = (\omega - \Omega) - \varepsilon\mu\frac{\Omega^2}{a\omega}\cos(\varphi + \psi)\cos\varphi$$
$$- \varepsilon\zeta\frac{\sin 2(\varphi + \psi)}{2}, \tag{2.65}$$

$$\dot{\Omega} = \varepsilon\gamma\mathcal{M}(\Omega) - \varepsilon\eta a\omega^2\cos(\varphi + \psi)\sin\varphi. \tag{2.66}$$

Equations (2.64)–(2.66) are three coupled strong nonlinear equations.

Averaging Procedure

For simplicity, let us introduce the averaging over the period of the trigonometric function φ for the period 2π. After averaging it is

$$\dot{a} = -\frac{1}{2}\varepsilon\zeta a - \frac{1}{2}\varepsilon\mu\frac{\Omega^2}{\omega}\sin\psi, \tag{2.67}$$

$$\dot{\psi} = (\omega - \Omega) - \frac{\varepsilon\mu\Omega^2}{2a\omega}\cos\psi, \tag{2.68}$$

$$\dot{\Omega} = \varepsilon\gamma\mathcal{M}(\dot{\varphi}) + \frac{1}{2}\varepsilon\eta a\omega^2\sin\psi. \tag{2.69}$$

For the steady state motion, when $\dot{a} = 0$, $\dot{\psi} = 0$ and $\dot{\Omega} = 0$, the Eqs. (2.67)–(2.69) transform into

$$\frac{\varepsilon\mu\Omega^2}{2\omega}\sin\psi = -\frac{1}{2}\varepsilon\zeta a, \tag{2.70}$$

$$\frac{\varepsilon\mu\Omega^2}{2\omega}\cos\psi = (\omega - \Omega)a, \tag{2.71}$$

$$\frac{1}{2}\varepsilon\eta a\omega^2\sin\psi = -\varepsilon\gamma\mathcal{M}(\dot{\varphi}). \tag{2.72}$$

Using relations (2.70) and (2.71) the amplitude -frequency relation is obtained

$$a = \frac{\varepsilon\mu\Omega^2}{\omega\sqrt{(\varepsilon\zeta)^2 + 4(\omega - \Omega)^2}}. \tag{2.73}$$

Eliminating ψ in the Eqs. (2.70) and (2.72), we have

$$\frac{(\varepsilon\eta)(\varepsilon\zeta)\omega^3}{2\varepsilon\mu\Omega^2}a^2 = \varepsilon\gamma\mathcal{M}(\dot{\varphi}) \equiv \varepsilon\gamma M_0\left(1 - \frac{\Omega}{\Omega_0}\right). \tag{2.74}$$

2.2.3   Comparison of the Systems with Constant and Variable Mass

Let us compare the properties of the systems with various values of mass. The characteristic points, which represent the intersection of curves (2.73) and (2.74), will be analyzed. In Fig. 2.11 the points of intersection of amplitude-frequency and characteristic curve are presented: in Fig. 2.11a the intersection of an amplitude-frequency curve and various characteristic curves and in Fig. 2.11b for one characteristic curve and amplitude-frequency curves for various values of mass are plotted.

In Fig. 2.11a the intersection of the amplitude-frequency diagram for $m_1 = m_{10}$ and various values of motor torque are plotted. It can be seen that there may be one or three points of intersection: two of them are stable and one is unstable. In Fig. 2.11b only one motor characteristic for $m_1 = m_{10}$ is plotted.

Namely, the influence of the small mass variation on the motor characteristic is negligible. The intersection of this motor characteristic and of amplitude-frequency diagrams obtained for various values of mass m_1 is plotted in Fig. 2.11b It is seen that for $m_1 = m_{10}$ there are three intersection points. If the mass is higher than m_{10}, i.e., $m_1 = 1.1m_{10}$, the amplitude-frequency diagram is moved to left the number of intersections decreases from three to only one. If the mass is smaller than m_{10}, i.e., $m_1 = 0.9m_{10}$, the amplitude-frequency diagram is moved to right in comparison to the previous one. There exists only one steady state position. It can be concluded that the value of mass has an influence on the number and position of characteristic points. Besides, it can be seen that the maximal amplitude depends on the non-dimensional damping coefficient, as it is affected with mass value: for the higher value of mass the maximal amplitude of vibration is smaller than for m_{10}. Otherwise, the smaller the mass, the higher the value of the maximal amplitude.

In Fig. 2.12a–c the influence of mass increase on the position of the characteristic point with small amplitude and high frequency is plotted. The amplitude of steady state position decreases from 1 to 3, while the frequency increases.
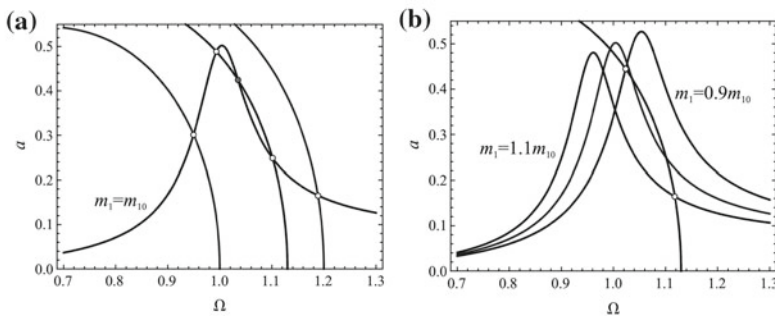

Fig. 2.11   a Intersection of the amplitude-frequency diagram and various values of motor torque; **b** Intersection of the motor torque and amplitude-frequency diagrams for various values of masses
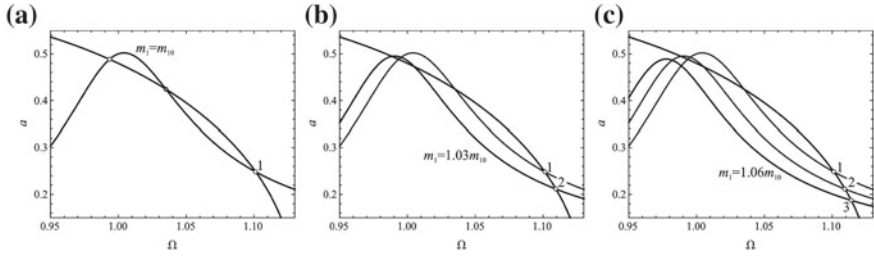
Fig. 2.12 The motion of the lower intersection point for increasing mass: **a** $m_1 = m_{10}$, **b** $m_1 = 1.03m_{10}$, **c** $m_1 = 1.06m_{10}$
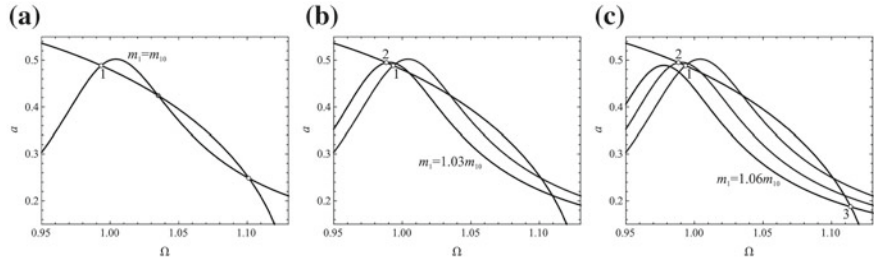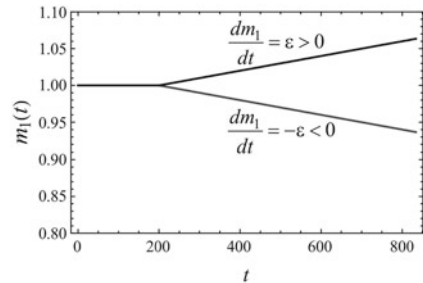

Fig. 2.13 The motion of the upper intersection point for increasing mass: **a** $m_1 = m_{10}$, **b** $m_1 = 1.03m_{10}$, **c** $m_1 = 1.06m_{10}$

Fig. 2.14 Mass-time diagrams

The second characteristic point which corresponds to the steady state motion also moves due to mass increase (see Fig. 2.13a–c). First the intersection point moves toward higher amplitude and smaller frequency (point 2) and then jumps to the position 3 with small amplitude and high frequency.

In Fig. 2.14 the mass-time diagrams are plotted: for $t \in [0, 200]$ the mass is constant, while for $t > 200$ mass is increasing ($\varepsilon > 0$) of decreasing ($\varepsilon < 0$). In Fig. 2.15 the displacement and frequency time history diagrams for mass increase are plotted.
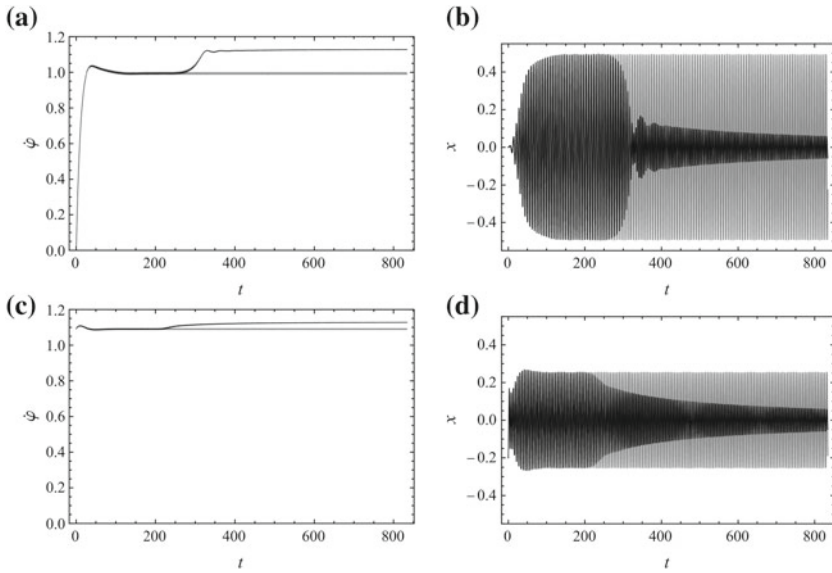
Fig. 2.15 a Frequency-time diagram for upper steady state position, **b** Displacement-time diagram for upper steady state position, **c** Frequency-time diagram for lower steady state position, **d** Displacement-time diagram for lower steady state position. Mass is constant (*gray line*) and mass is increasing (*black mass*)

In Fig. 2.15a the frequency-time diagram for upper steady state position is plotted. For the constant mass after the transient motion the frequency is constant. If the mass is increasing the frequency increase, too. In Fig. 2.15b the displacement-time diagram for upper steady state position and constant mass is the gray line. Increasing the mass the amplitude decreases with mass increase. The same tendency of motion is evident for the lower steady state position (Fig. 2.15c, d). In Fig. 2.16 the case when the mass is decreasing is plotted. For the case when the mass is constant the displacement-time (gray line) and frequency-time diagrams are constant, while for decreasing mass the frequency-time diagrams decrease (Fig. 2.16a, c). Decrease of mass causes the displacement-time diagram (black line) for the upper position to decrease (Fig. 2.16b) while for the lower position to increase (Fig. 2.16d).

Finally, it can be concluded that the mass variation is suitable to be applied as a method for control of motion in non-ideal systems.
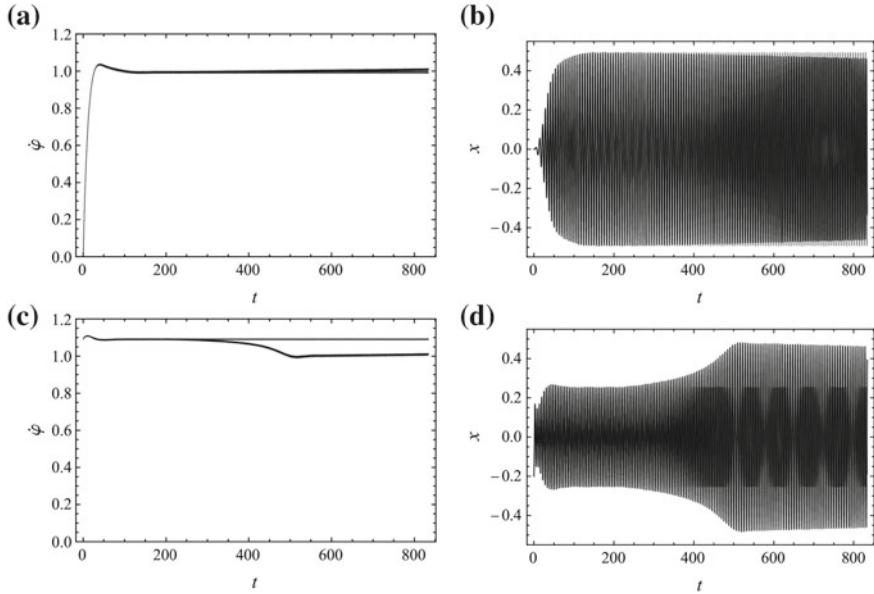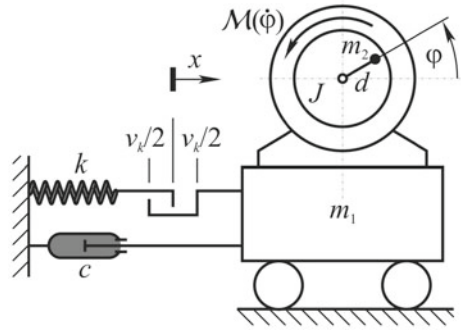
Fig. 2.16 a Frequency-time diagram for upper steady state position, **b** Displacement-time diagram for upper steady state position, **c** Frequency-time diagram for lower steady state position, **d** Displacement-time diagram for lower steady state position. Mass is constant (*black line*) and mass is decreasing (*gray mass*)

2.3 Oscillator with Clearance Coupled with a Non-ideal Source

In the previous sections we discussed the cases when the connection between the oscillator and the fixed element is continual. Introducing the clearance in the connection between the oscillator and the fixed element, the discontinual elastic force acts. It has to be mentioned that the elastic property is a linear displacement function, but due to discontinuity the system may be treated as the nonlinear one. The mathematical model of the system is given with two coupled nonlinear differential equations. For the case of small nonlinearity the asymptotic methods are applied for determining of the transient and steady-state motion and their stability. In the system the Sommerfeld effect occurs. Beside the regular, the chaotic motion in non-ideal mechanical systems with clearance exists. It is of interest to obtain conditions for transformation of the chaotic motion into periodic motion (Zukovic and Cveticanin 2009).

2.3.1 Model of the System

The non-ideal system with clearance is modeled as an oscillatory system with unbalanced motor (Fig. 2.17).

The mechanical model contains the oscillatory mass m_1 and the motor with moment of inertia J, unbalance m_2 and eccentricity d. The connection of the oscillator to the fixed element has the rigidity k, damping c and clearance v_k. The excitation torque of the motor, $\mathcal{M}(\dot{\varphi})$, is the function of the angular velocity $\dot{\varphi}$

$$\mathcal{M}(\dot{\varphi}) = M_0\left(1 - \frac{\dot{\varphi}}{\Omega_0}\right),\tag{2.75}$$

where Ω_0 is the steady-state angular velocity. This mathematical model corresponds to asynchronous AC motor (Dimentberg et al. 1997).

For the generalized coordinates: the displacement of the oscillator x and the rotation angle of the motor φ, the motion of the system is described with a system of two coupled non-linear differential equations

$$(m_1 + m_2)\,\ddot{x} + c\dot{x} + F_k = m_2 d\left(\ddot{\varphi}\sin\varphi + \dot{\varphi}^2\cos\varphi\right),$$
$$\left(J + m_2 d^2\right)\ddot{\varphi} = m_2 d\ddot{x}\sin\varphi + \mathcal{M}(\dot{\varphi}),\tag{2.76}$$

where F_k is the elastic force in the spring. The weight of the elements is neglected as the motion of the system is in horizontal plane.

For the clearance v_k, the spring has not an influence on the motion of the system as the elastic force F_k is zero (Fig. 2.18a).

For the case of spring extension it is assumed that the elastic force is the linear displacement function

$$F_k(x) = kx + f_k = kx + \begin{cases} -k\frac{v_k}{2} & \text{if} & x > \frac{v_k}{2} \\ -kx & \text{if} & -\frac{v_k}{2} \le x \le \frac{v_k}{2} \\ k\frac{v_k}{2} & \text{if} & x < -\frac{v_k}{2} \end{cases}.\tag{2.77}$$
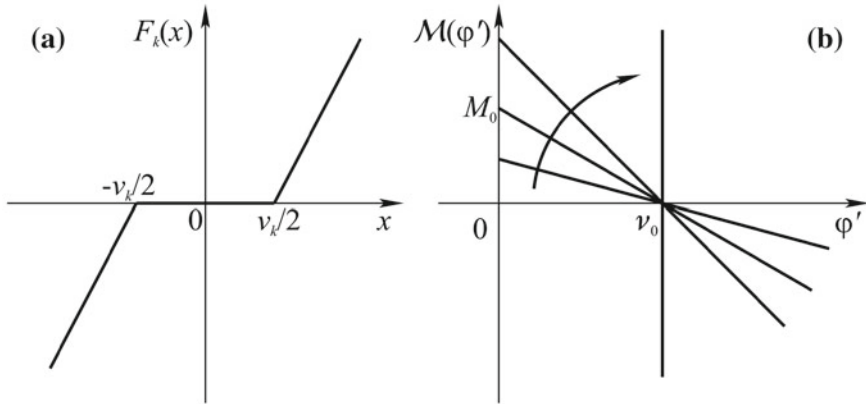
Fig. 2.18 Properties of the system: **a** elastic force distribution, **b** motor-torque characteristics

where kx is the linear part of the force and f_k is different in the interval in front of and beyond clearance and also in the clearance.

By introducing the dimensionless displacement

$$y = \frac{x}{d},\tag{2.78}$$

and dimensionless time

$$\tau = \omega t,\tag{2.79}$$

and also (2.77) into (2.76), the dimensionless differential equations of motion of the oscillatory system are obtained

$$\begin{aligned} y'' + y &= -\zeta y' - \kappa f_k + \mu \left(\varphi'' \sin \varphi + \varphi'^2 \cos \varphi \right), \\ \varphi'' &= \eta y'' \sin \varphi + \xi\, \mathcal{M} \left(\varphi' \right), \end{aligned}\tag{2.80}$$

where $\omega = \sqrt{\frac{k}{m_1+m_2}}$ is the eigenfrequency of the system, $(') \equiv d/d\tau$ and

$$\zeta = \frac{c}{\sqrt{k\,(m_1+m_2)}}, \quad \kappa = \frac{1}{dk}, \quad \mu = \frac{m_2}{(m_1+m_2)},$$

$$\eta = \frac{m_2 d^2}{\left(J + m_2 d^2\right)}, \quad \xi = \frac{1}{\omega^2 \left(J + m_2 d^2\right)}.\tag{2.81}$$

The dimensionless elastic force is

$$\kappa f_k(y) = \begin{cases} -\frac{V_k}{2} & if & y > \frac{V_k}{2} \\ -y & if & -\frac{V_k}{2} \le y \le \frac{V_k}{2} \\ \frac{V_k}{2} & if & y < -\frac{V_k}{2} \end{cases}, \tag{2.82}$$

where $V_k = \frac{v_k}{d}$ is the dimensionless clearance. In dimensionless coordinates the torque is the function of the dimensionless angular velocity φ'

$$\mathcal{M}(\varphi') = M_0 \left(1 - \frac{\varphi'}{\nu_0} \right) \tag{2.83}$$

where $\nu_0 = \frac{\Omega_0}{\omega}$. The parameter M_0 has a significant influence on the gradient of the curve (see Fig. 2.18b): for higher values of parameter the gradient is higher and tends to vertical position when the power is unlimited and the system is ideal.

2.3.2 Transient Motion of the System

The motion of the system, with small nonlinearity and energy supply close to ideal, is considered. Due to real properties of the system it can be concluded that the parameters α, μ, κ, η and ξ in (2.80) are small. The parameters are described as

$$\zeta = \varepsilon\zeta_1, \qquad \mu = \varepsilon\mu_1, \qquad \eta = \varepsilon\eta_1, \qquad \xi = \varepsilon\xi_1, \tag{2.84}$$

where $\varepsilon << 1$ is a small parameter.

For (2.84) the differential equations of motion (2.80) are transformed into

$$\begin{aligned} y'' + y &= -\varepsilon\alpha_1 y' + \varepsilon\mu_1 \left(\varphi'' \sin\varphi + \varphi'^2 \cos\varphi \right) - \kappa f_k, \\ \varphi'' &= \varepsilon\eta_1 y'' \sin\varphi + \varepsilon\xi_1 \mathcal{M}(\varphi'), \end{aligned} \tag{2.85}$$

where $(') \equiv (d/d\tau)$ and $('') \equiv (d^2/d\tau^2)$. After some simplification and neglecting the second order small values in (2.85) the following system of differential equations of motion is obtained

$$\begin{aligned} y'' + y &= -\varepsilon\zeta_1 y' + \varepsilon\mu_1 \varphi'^2 \cos\varphi - \kappa f_k, \\ \varphi'' &= -\varepsilon\eta_1 y \sin\varphi + \varepsilon\xi_1 \mathcal{M}(\varphi'). \end{aligned} \tag{2.86}$$

Substituting (2.82) and (2.83) into (2.86), neglecting the damping term and assuming that the clearance is small, i.e., $y \gtrless \frac{\varepsilon V_k}{2}$, it follows

$$y'' + y = \varepsilon \mu_1 \varphi'^2 \cos \varphi \pm \frac{\varepsilon V_k}{2},$$

$$\varphi'' = -\varepsilon \eta_1 y \sin \varphi + \varepsilon \xi_1 M_0 \left(1 - \frac{\varphi'}{\nu_0} \right) \quad for \quad y \gtrless \frac{\varepsilon V_k}{2}. \qquad (2.87)$$

Analyzing the first relation in (2.87), it is concluded that for

$$-\frac{\varepsilon V_k}{2} \le y \le \frac{\varepsilon V_k}{2},$$

the deflection y is of order $O(\varepsilon)$ and that the first term on the right side of the second equation is a small value of order $O(\varepsilon^2)$. Neglecting the second order small values, it follows

$$y'' = \varepsilon \mu_1 \varphi'^2 \cos \varphi,$$

$$\varphi'' = \varepsilon \xi_1 M_0 \left(1 - \frac{\varphi'}{\nu_0} \right) \quad for \quad -\frac{\varepsilon V_k}{2} \le y \le \frac{\varepsilon V_k}{2}. \qquad (2.88)$$

Introducing the series expansion

$$y = y_0 + \varepsilon y_1 + \cdots, \qquad \varphi = \varphi_0 + \varepsilon \varphi_1 + \cdots, \qquad (2.89)$$

into (2.87), and separating the terms with the same order of small parameter ε the following system of differential equations is obtained

$$\varepsilon^0 \quad : \qquad y_0'' + y_0 = 0, \qquad \varphi_0'' = 0, \qquad (2.90)$$

$$\varepsilon^1 \quad : \qquad y_1'' + y_1 = \mu_1 \left(\varphi_0' \right)^2 \cos \varphi_0 \mp \frac{V_k}{2}, \qquad (2.91)$$

$$\varphi_1'' = -\eta_1 y_0 \sin \varphi_0 + \xi_1 M_0 \left(1 - \frac{\varphi_0'}{\nu_0} \right),$$

$$\cdots$$

with initial conditions

$$\varepsilon^0 \quad : \qquad y_0(\tau_0) = Y_0, \quad y_0'(\tau_0) = Y_0', \quad \varphi_0(\tau_0) = \Phi_0, \quad \varphi_0'(\tau_0) = \Phi_0',$$
$$(2.92)$$

$$\varepsilon^1 \quad : \qquad y_1(\tau_0) = 0, \quad y_1'(\tau_0) = 0, \quad \varphi_1(\tau_0) = 0, \quad \varphi_1'(\tau_0) = 0, \qquad (2.93)$$

$$\cdots$$

The solution of (2.90) is

$$y_0 = A_0 \cos(\tau + \alpha_0), \qquad \varphi_0 = B_0 \tau + C_0, \qquad (2.94)$$

and of (2.91)

$$y_1 = A_1 \cos(\tau + \alpha_1) \mp \frac{V_k}{2} + \frac{\mu_1 B_0^2}{1 - B_0^2} \cos(B_0 \tau + C_0), \tag{2.95}$$

$$\varphi_1 = \frac{(1 - B_0)^2}{2} \eta_1 A_0 \sin[(1 - B_0)\tau + (\alpha_0 - C_0)]$$

$$+ \frac{(1 + B_0)^2}{2} \eta_1 A_0 \sin[(1 + B_0)\tau$$

$$+ (\alpha_0 + C_0)] + \xi_1 M_0 \left(1 - \frac{B_0}{\nu_0}\right) \frac{\tau^2}{2} + B_1 \tau + C_1, \tag{2.96}$$

where A_0, B_0, C_0 and α_0 are integrating constants which have to be determined according to (2.92), and A_1, B_1, C_1 and α_1 according to (2.93). In general, the solution in the first approximation for the case when the elastic force acts is

$$y = A_0 \cos(\tau + \alpha_0) + \varepsilon A_1 \cos(\tau + \alpha_1)$$

$$\mp \frac{\varepsilon V_k}{2} + \frac{\varepsilon \mu_1 B_0^2}{1 - B_0^2} \cos(B_0 \tau + C_0), \tag{2.97}$$

$$\varphi = (B_0 + \varepsilon B_1)\tau + (C_0 + \varepsilon C_1) + \varepsilon \xi_1 M_0 \left(1 - \frac{B_0}{\nu_0}\right) \frac{\tau^2}{2}$$

$$+ \frac{\varepsilon \eta_1 A_0}{2(1 - B_0)^2} \sin[(1 - B_0)\tau + (\alpha_0 - C_0)] \tag{2.98}$$

$$+ \frac{\varepsilon \eta_1 A_0}{2(1 + B_0)^2} \sin[(1 + B_0)\tau + (\alpha_0 + C_0)],$$

and

$$y' = -A_0 \sin(\tau + \alpha_0) - \left[\varepsilon A_1 \sin(\tau + \alpha_0) + \frac{\varepsilon \mu_1 B_0^3}{1 - B_0^2} \sin(B_0 \tau + C_0)\right], \tag{2.99}$$

$$\varphi' = B_0 + \varepsilon B_1 + \varepsilon \xi_1 M_0 \left(1 - \frac{B_0}{\nu_0}\right) \tau + \frac{\varepsilon \eta_1 A_0}{2(1 - B_0)} \cos[(1 - B_0)\tau + (\alpha_0 - C_0)]$$

$$+ \frac{\varepsilon \eta_1 A_0}{2(1 + B_0)} \cos[(1 + B_0)\tau + (\alpha_0 + C_0)]. \tag{2.100}$$

For the deflection $y = (\mp \varepsilon V_k/2)$ using (2.97) the value of time τ_V is calculated. Substituting this value of time τ_V into (2.98)–(2.100) the position and velocities $\varphi(\tau_v)$, $y'(\tau_v)$ and $\varphi'(\tau_v)$ are determined. The values

$$y(\tau_v) = \mp \varepsilon V_k/2, \qquad y'(\tau_v), \ \varphi(\tau_v), \ \varphi'(\tau_v), \tag{2.101}$$

are the initial conditions for the motion of the system without elastic force. According to (2.88)

$$\varphi = K_0 + \nu_0\tau + \frac{\nu_0^2 K_1}{\varepsilon\xi_1 M_0}\exp\left(-\frac{\varepsilon\xi_1 M_0\tau}{\nu_0}\right) \tag{2.102}$$

$$\approx \left(K_0 + \frac{\nu_0^2 K_1}{\varepsilon\xi_1 M_0}\right) + \nu_0(1 - K_1)\tau,$$

$$\varphi' = \nu_0 - \nu_0 K_1\exp\left(-\frac{\varepsilon\xi_1 M_0\tau}{\nu_0}\right) \approx \nu_0(1 - K_1) + K_1\varepsilon\xi_1 M_0\tau, \tag{2.103}$$

$$y = -\varepsilon\mu_1\cos\left[\left(K_0 + \frac{\nu_0^2 K_1}{\varepsilon\xi_1 M_0}\right) + \nu_0(1 - K_1)\tau\right] + K_2\tau + K_3, \tag{2.104}$$

$$y' = K_2 + \varepsilon\mu_1\nu_0(1 - K_1)\sin\left[\left(K_0 + \frac{\nu_0^2 K_1}{\varepsilon\xi_1 M_0}\right) + \nu_0(1 - K_1)\tau\right], \tag{2.105}$$

where the constants K_0, K_1, K_2 and K_3 depend on the initial conditions (2.101). The elastic force acts when $y = (\pm\varepsilon V_k/2)$ and the motion functions are (2.97)–(2.100) with initial conditions which correspond to τ and (2.103)–(2.105) at that displacement position.

In Fig. 2.19 the $y - \tau$, $y' - \tau$, $\varphi - \tau$ and $\varphi' - \tau$ time history diagrams for $\zeta_1 = 0$, $\mu_1 = 1$, $\eta_1 = 1$, $\xi_1 = 0.5$, $\nu_0 = 1.1$, $\varepsilon = 0.1$. and initial conditions $y(0) = 0.5$,
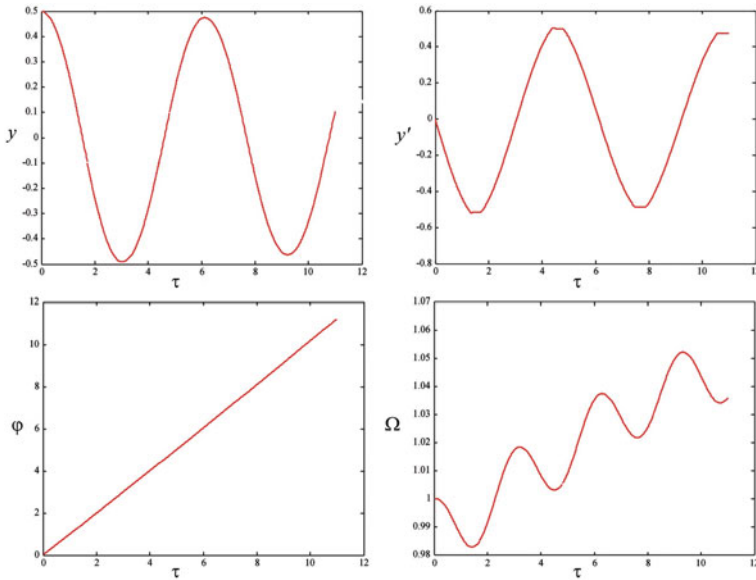

Fig. 2.19 Time-history diagrams: **a** $y - \tau$, **b** $y' - \tau$, **c** $\varphi - \tau$, **d** $\Omega - \tau$, for $V_k = 0.1$, $\mu_1 = 1$, $\eta_1 = 1$, $\xi_1 = 0.5$, $\nu_0 = 1.1$, $\varepsilon = 0.1$ and initial conditions $y(0) = 0.5$, $y'(0) = 0$, $\varphi(0) = 0$, $\varphi'(0) = 1$

$y'(0) = 0$, $\varphi(0) = 0$, $\varphi'(0) = 1$ are plotted. Analytical solutions obtained by solving Eqs. (2.87) and (2.88) are shown. Due to small parameter values and a short time period the differences between the solutions are negligible.

2.3.3 Steady-State Motion of the System

The system of non-linear equations (2.86) is approximately solved by applying of the well known Krylov–Bogolyubov method of slow variable amplitude and phase (Bogolyubov and Mitropolskij 1974). For $\varepsilon = 0$ the solution is

$$y = a \cos(\varphi + \psi), \qquad \varphi' = \Omega = const., \tag{2.106}$$

where a, φ and ψ are the amplitude, frequency and phase of vibration and Ω is the constant angular velocity. Based on (2.106) the approximate solution is

$$y(\tau) = a(\tau) \cos(\varphi(\tau) + \psi(\tau)), \qquad \varphi' = \Omega(\tau), \tag{2.107}$$

where the amplitude $a = a(\tau)$, phase $\psi = \psi(\tau)$ and excitation frequency $\varphi'(\tau)$ are functions of slow time τ. The first time derivative of (2.107) is

$$y'(\tau) = -a \sin(\varphi + \psi,) \tag{2.108}$$

when

$$\psi' = (1 - \Omega) + \frac{a'}{a} \frac{\cos(\varphi + \psi)}{\sin(\varphi + \psi)}. \tag{2.109}$$

The time derivative of (2.108) is

$$y'' = -a' \sin(\varphi + \psi) - a\Omega \cos(\varphi + \psi) - a\psi' \cos(\varphi + \psi). \tag{2.110}$$

Substituting (2.107)–(2.110) into (2.86) the differential equations with new variables A, ψ and Ω are obtained

$$a' = - \left(\varepsilon \zeta_1 a \sin(\varphi + \psi) + \varepsilon \mu_1 \Omega^2 \cos\varphi \right) \sin(\varphi + \psi) + \varepsilon \, \kappa_1 \, f_k \sin(\varphi + \psi) \equiv g_A,$$

$$\psi' = (\Omega - 1) - \frac{\cos(\varphi + \psi)}{a} \left(\varepsilon \zeta_1 a \sin(\varphi + \psi) + \varepsilon \mu_1 \Omega^2 \cos\varphi \right)$$

$$\quad + \frac{\cos(\varphi + \psi)}{a} \varepsilon \kappa_1 \, f_k$$

$$\quad \equiv g_\psi,$$

$$\Omega' = -\varepsilon \eta_1 a \cos(\varphi + \psi) \sin\varphi + \varepsilon \xi_1 \, \mathcal{M}(\Omega) \equiv g_\Omega. \tag{2.111}$$

To solve the system of coupled equations (2.111) is not an easy task. Due to the fact that the functions g_A, g_ψ and g_Ω are periodical, the averaging procedure is introduced. The averaged differential equations (2.111) are

$$a' = \frac{1}{2\pi} \int_0^{2\pi} g_A d\varphi = -\frac{1}{2} \left(\varepsilon \zeta_1 a + \varepsilon \mu_1 \Omega^2 \sin \psi \right) + G_A,$$

$$\psi' = \frac{1}{2\pi} \int_0^{2\pi} g_\psi d\varphi = 1 - \Omega - \frac{\varepsilon \mu_1}{2a} \Omega^2 \cos \psi + G_\psi, \qquad (2.112)$$

$$\Omega' = \frac{1}{2\pi} \int_0^{2\pi} g_\Omega d\varphi = \frac{1}{2} \varepsilon \eta_1 a \sin \psi + \varepsilon \xi_1 \mathcal{M} (\Omega).$$

For $a > V_k/2$

$$G_A = \frac{1}{2\pi} \int_0^{2\pi} \left(\varepsilon (\sin (\varphi + \psi)) (\kappa_1 f_k) \right) d\varphi = 0,$$

$$G_\psi = \frac{1}{2\pi} \int_0^{2\pi} \left(\varepsilon \frac{1}{a} (\cos (\varphi + \psi)) (\kappa_1 f_k) \right) d\varphi \qquad (2.113)$$

$$= \frac{1}{\pi} \left(-\frac{V_k}{2a} \sqrt{1 - \left(\frac{V_k}{2a} \right)^2} + \arccos \frac{V_k}{2a} \right) + \left(-\frac{1}{2} \right),$$

and for $a \leq V_k/2$ when the elastic force is zero

$$G_A = 0, \qquad G_\psi = -\frac{1}{2}. \qquad (2.114)$$

For the steady-state motion, when $a = const.$, $\psi = const.$ and $\Omega = const.$, the differential equations (2.112) simplify to

$$\varepsilon \zeta_1 a + \varepsilon \mu_1 \Omega^2 \sin \psi = 0, \qquad (2.115)$$

$$\left(1 - \Omega - \frac{\varepsilon \mu_1}{2a} \Omega^2 \cos \psi \right) + G_\psi = 0, \qquad (2.116)$$

$$\frac{1}{2} \varepsilon \eta_1 a \sin \psi + \varepsilon \xi_1 \mathcal{M} (\Omega) = 0. \qquad (2.117)$$

From (2.115) and (2.116) the A - Ω relation is obtained

$$A = \frac{\varepsilon \mu_1 \Omega^2}{\sqrt{\varepsilon^2 \alpha_1^2 + 4\left(1 - \Omega + G_\psi\right)^2}}. \qquad (2.118)$$

For $a > V_k/2$ the amplitude-frequency function depends on the clearance, i.e.,

$$a = \frac{\varepsilon \mu_1 \Omega^2}{\sqrt{\varepsilon^2 \zeta_1^2 + \left(1 - 2\Omega - \frac{V_k}{a\pi}\sqrt{1 - \left(\frac{V_k}{2a}\right)^2} + \frac{2}{\pi}\arccos\frac{V_k}{2a}\right)^2}}. \qquad (2.119)$$

For $a = V_k/2$, the amplitude-frequency function is

$$a = \frac{\varepsilon \mu_1 \Omega^2}{\sqrt{(1 - 2\Omega)^2 + \varepsilon^2 \zeta_1^2}}. \qquad (2.120)$$

The relation is independent on the value of the clearance.

The amplitude has the extreme value for

$$\Omega = \frac{1-p}{4}\left(3 \pm \sqrt{1 - \frac{8\varepsilon^2 \zeta_1^2}{(1-p)^2}}\right), \qquad (2.121)$$

where

$$p = \frac{2}{\pi}\arccos\frac{V_k}{2a} - \frac{V_k}{a\pi}\sqrt{1 - \left(\frac{V_k}{2a}\right)^2}. \qquad (2.122)$$

If $a = V_k/2$ and

$$\Omega = \frac{1}{4}(3 \pm \sqrt{1 - 8\varepsilon^2 \zeta_1^2}), \qquad (2.123)$$

the maximal amplitude is

$$a = \varepsilon \mu_1 \frac{(5 - 3\sqrt{1 - 8\varepsilon^2\zeta_1^2} - 4\varepsilon^2\zeta_1^2)}{4\sqrt{2 - 2\sqrt{1 - 8\varepsilon^2\zeta_1^2} - 4\varepsilon^2\zeta_1^2}} \approx \varepsilon \mu_1 \frac{1 + 4\varepsilon^2\zeta_1^2}{4\sqrt{2}\varepsilon^2\zeta_1^2}. \qquad (2.124)$$

The maximal amplitude depends on the damping properties of the system and mass distribution in the system. For extremely small ζ_1, when the damping is negligible, the maximal value of the amplitude a tends to infinity for $\Omega = 1/2$.

Fig. 2.20 Amplitude-
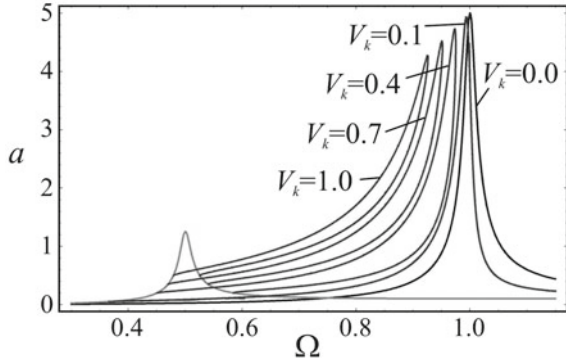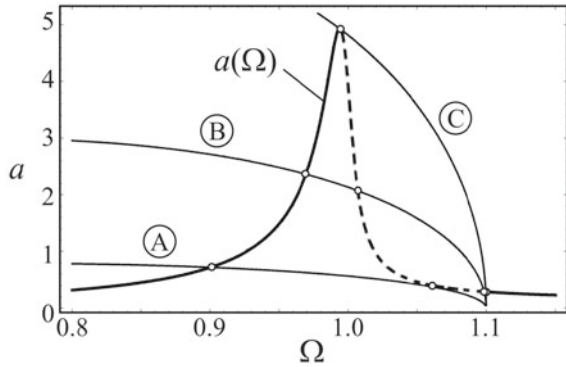frequency curves for various
values of clearance

Fig. 2.21 Frequency-
response curve and
characteristics of the motor:
stable (——) and unstable
(- - -) solutions

In Fig. 2.20 the amplitude-frequency diagrams for various values of clearance V_k
are plotted. The parameters of the system are $\varepsilon\zeta_1 = 0.02$, $\varepsilon\mu_1 = 0.1$, $\varepsilon\eta_1 = 0.1$,
$\varepsilon\xi_1 = 0.05$, $\nu_0 = 1.1$ and $\varepsilon = 0.1$.

Using the characteristics of the motor (2.83) and the relations (2.115) and (2.117),
we obtain the following relation

$$M_0 \left(1 - \frac{\Omega}{\nu_0}\right) \Omega^2 = \frac{1}{2} \frac{\zeta_1 \eta_1}{\mu_1 \xi_1} a^2. \qquad (2.125)$$

Solving the Eqs. (2.118) and (2.125), we obtain the approximate values of the
steady-state amplitude a and angular velocity of motor Ω.

In Fig. 2.21, for parameter values $\zeta_1 = 0.2$, $\mu_1 = 1$, $\eta_1 = 1$, $\xi_1 = 0.5$, $\nu_0 = 1.1$,
$\varepsilon = 0.1$ and $V_k = 0.1$, the frequency-response curve is plotted. The intersection
between the motor characteristic (A, B, C) and the curve defines the number of the
steady-state motions. For the two boundary curves A and C the number of steady-
state solutions is two. Inside the boundary curves A and C there are three steady-
state solutions (for example for the curve B). Outside the boundary curves only one

steady-state solution exists: for small values of M_0 (below the curve A), and for very high values of M_0 (above curve C).

Which of steady-state motion will be realized depends on the stability and initial conditions. For stability analysis the perturbed amplitude, phase and frequency, $a = a_S + a_1, \psi = \psi_S + \psi_1$ and $\Omega = \Omega_S + \Omega_1$, are considered, where a_S, ψ_S and Ω_s are the steady-state values and a_1, ψ_1 and Ω_1 the perturbations. The linearized differential equations with perturbed values are

$$a_1' = -\frac{1}{2}\varepsilon\zeta_1 a_1 - \frac{1}{2}\varepsilon\mu_1\Omega_S^2\cos(\psi_S)\psi_1 - \varepsilon\mu_1\Omega_S\sin(\psi_S)\Omega_1,$$

$$\psi_1' = \left(\frac{1}{2}\varepsilon\mu_1\Omega_S^2\frac{\cos(\psi_S)}{a_S^2} + \left(\frac{\partial G_\psi}{\partial a}\right)_S\right)a_1 + \frac{1}{2}\frac{\varepsilon}{a_S}\mu_1\Omega_S^2\sin(\psi_S)\psi_1$$
$$+ \left(-1 - \frac{\varepsilon\mu_1}{a}\Omega_S\cos(\psi_S)\right)\Omega_1,$$

$$\Omega_1' = \frac{a_1}{2}\varepsilon\eta_1\sin(\psi_S) + \frac{\psi_1}{2}\varepsilon\eta_1 a_S\cos(\psi_S) + \varepsilon\xi_1\Omega_1\left(\frac{\partial\mathcal{M}(\Omega)}{\partial\Omega}\right)_S, \quad (2.126)$$

where $\frac{\partial G_\psi}{\partial a} = \frac{1}{\pi}\frac{V_k}{a^2}\sqrt{1 - \left(\frac{V_k}{2a}\right)^2}$ and $\frac{\partial\mathcal{M}(\Omega)}{\partial\Omega} = -\frac{M_0}{\nu_0}$, and $(\cdot)_S$ is the notation for steady-state condition. Using the Routh–Hurwitz procedure the stability is investigated. In Fig. 2.21, the stability regions in frequency-response diagram are plotted. The dot line is used for the unstable solutions.
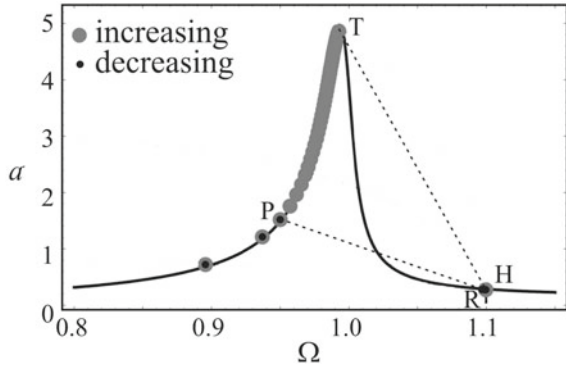
To prove the correctness of the previous mentioned analytical procedure the approximate analytical solutions are compared with 'exact' numerical solutions. The system of two differential equations (2.80) is transformed into four first order differential equations

$$y_1' = y_2,$$
$$y_2' = \frac{1}{\left(1 - \mu\eta\sin^2 y_3\right)}\left(-y_1 - \zeta y_2 + \mu\left(\xi\mathcal{M}(y_4)\sin y_3 + y_4^2\cos y_3\right) - \kappa f_k\right),$$
$$y_3' = y_4, \quad (2.127)$$
$$y_4' = \frac{\eta\sin y_3\left(-y_1 - \zeta y_2 + \mu\left(\xi\mathcal{M}\sin y_3 + y_4^2\cos y_3\right) - \kappa f_k\right)}{\left(1 - \mu\eta\sin^2 y_3\right)} + \xi\mathcal{M},$$

where $y_1 = y, y_2 = y', y_3 = \varphi, y_4 = \varphi'$ and $\mathcal{M} = \mathcal{M}(y_4)$. The system of differential equations (2.127) is numerically solved by applying the Runge–Kutta method. The analytical and numerical solutions are plotted in Fig. 2.22.

It can be seen that the system cannot be made to respond at a frequency between Ω_T and Ω_H (grey points) and also Ω_R and Ω_P (black points) by increasing and decreasing of the control parameter M_0, respectively. This phenomena is called the Sommerfeld effect.

2.3.4 Chaotic Motion

Changing the control parameter M_0 the influence of motor properties on the system motion are numerically analyzed. The constant parameters of the system are: $\zeta = 0.04$, $\mu = .9375$, $\eta = 0.1$, $\xi = 0.5$, $\nu_0 = 0.2$ and $V_k = 0.01$.

For $M_0 = 0.35$ the motion of the system is periodical with period equal to excitation period (Fig. 2.23a). For control parameter $M_0 = 0.43$ the motion is periodic with period equal to double excitation period (Fig. 2.23b). Increasing the control parameter M_0 causes periodic motions with period doubling, as shown in bifurcation diagram (Fig. 2.24).

The multiplied bifurcations give the chaotic motion. It is concluded that for high values of control parameter ($M_0 > 75$), when the system tends to ideal one, the motion is chaotic. In Fig. 2.25 the phase plane for $M_0 = 100$ is plotted.
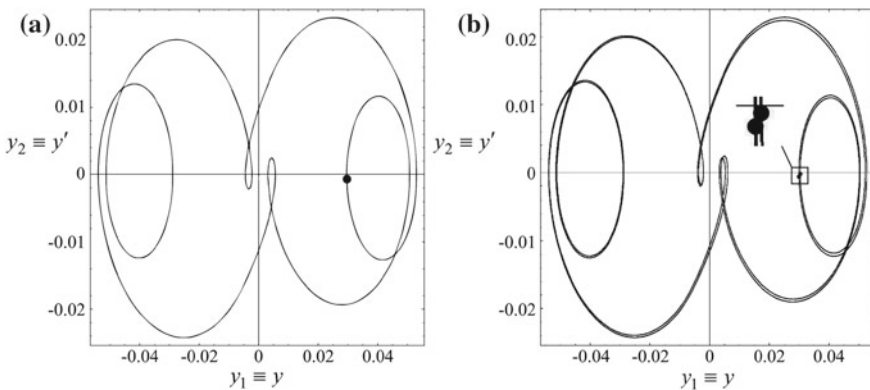

Fig. 2.23 Periodic motion: **a** period 1, **b** period 2

Fig. 2.24 Bifurcation diagram for control parameter M_0
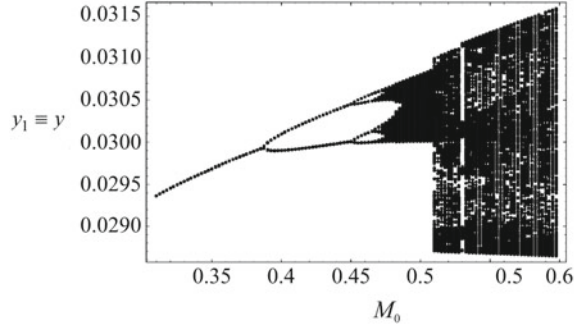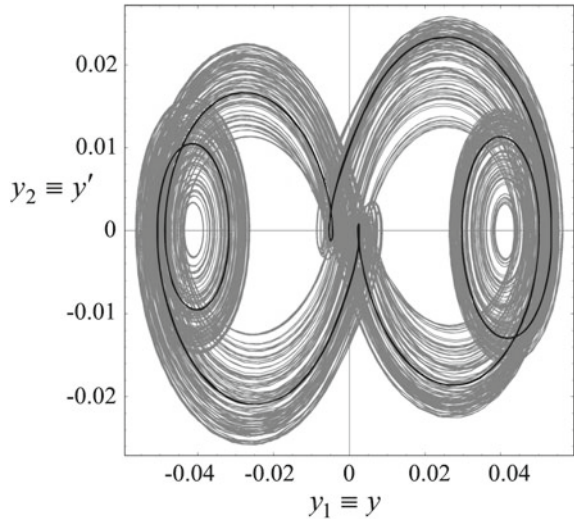

Fig. 2.25 Phase portrait for $M_0 = 100$: before chaos control (*grey line*) and after chaos control (*black line*)

To prove the existence of the chaotic motion the Lyapunov exponent is calculated. Using the procedures suggested by Wolf (1984) and Wolf et al. (1985), and also by Sandri (1996) the maximal Lyapunov exponent for chaotic motion is $\lambda = 0.0284$ (see Fig. 2.26).

The parameter k represents the number of periods of vibrations.

For the case when the control parameter is the clearance V_k the bifurcation diagram is plotted (see Fig. 2.27).

The parameters of the system are: $\alpha = 0.04$, $\mu = .9375$, $\eta = 0.1$, $\xi = 0.5$, $\nu_0 = 0.2$ and $M_0 = 10$. For the small values of clearance ($V_k \leqslant 0.005$) and for high values of clearance ($V_k \geqslant 0.2$) the period one motion occurs. In some regions of the interval $0.005 < V_k < 0.2$ even chaotic motion appears.
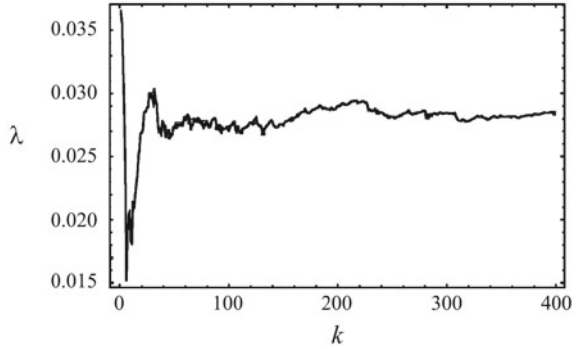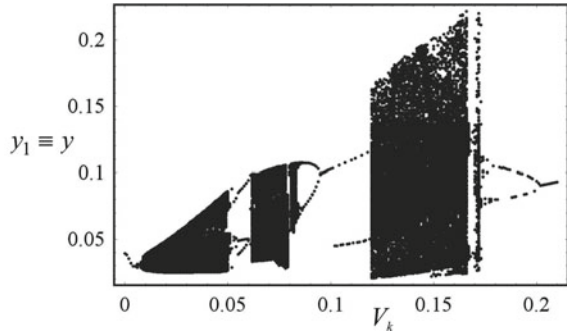
Fig. 2.26 Distribution of
Lyapunov exponent

Fig. 2.27 Bifurcation
diagram for control
parameter V_k

2.3.5 Chaos Control

Based on the known methods of chaos control (Ott et al. 1990; Pyragas 1992, 1996;
Alvarez-Ramirez et al. 2003; Tereshko et al. 2004; Balthazar and Brasil 2004), the
following control function is introduced

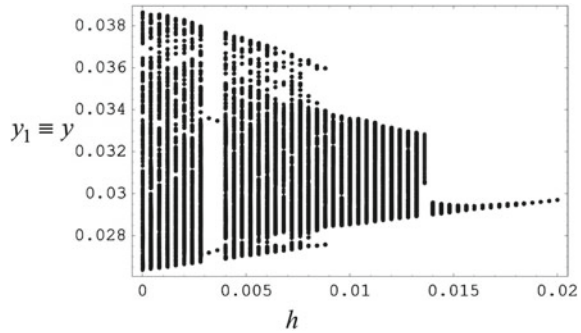$$g\left(y'\right) = -h \, \tanh\left(\chi \, y'\right), \tag{2.128}$$

where y' is dimensionless velocity of oscillator, h is the amplitude and χ the gradient
of the control function.

Solving the system of coupled differential equations of motion (2.80) with addition
of the control function (2.128)

$$y'' + y = -\alpha y' - \kappa f_k + \mu\left(\varphi'' \sin \varphi + \left(\varphi'\right)^2 \cos \varphi\right) - h \, \tanh\left(\chi \, y'\right),$$
$$\varphi'' = \eta y'' \sin \varphi + \xi \, \mathcal{M}\left(\varphi'\right), \tag{2.129}$$

the properties of the controlled system are obtained. The black line in Fig. 2.25 shows
the motion of the system after chaos control. The chaotic attractor is transformed
into periodic attractor for $\chi = 0.15$ and $h = 0.02$.

Fig. 2.28 Bifurcation
diagram after chaos control

It is worth to say that the applied control function is not an unique one, i.e., the chaos control is possible for various parameters of control function. In Fig. 2.28, the bifurcation diagram for the constant value of parameter value $\chi = 0.15$ and variable value of parameter h is plotted. It is obvious that the control of chaos and its transformation to periodic solution is possible for $h > 0.014$, and to periodic motion with period 1 for $h > 0.019$.

2.4   Conclusion

The most important results of the chapter can be expressed as:

1. In the non-ideal mechanical system which contains a non-ideal source and a linear oscillator or an oscillator with clearance the Sommerfeld effect is evident. In amplitude-frequency diagram the jump phenomena occurs. For certain values of frequencies there are no steady-state positions.

2. In spite of the fact that the elastic force is linear, the clearance causes the bending of the amplitude-frequency curve: the higher the value of the clearance, the bending is more significant.

3. Due to clearance the motion is continual but divided into intervals with and without elastic force. It causes the disturbance of the periodic motion.

4. For certain system parameters chaotic motion occur. The type of the steady-state motion depends not only on the torque but also on the value of the clearance in the system.

5. The chaos control based on the function which depends on the velocity of oscillator vibration is very convenient for non-ideal mechanical systems with clearance. The control is directed onto the oscillator and not on the motor as it is usually done.

6. Analog model is very appropriate to give an explanation of the dynamics of the resonance capture effect and can help students and young researchers to understand this phenomenon.

References

Alvarez-Ramirez, J., Espinosa-Paredes, G., & Puebla, H. (2003). Chaos control using small-amplitude damping signals. *Physics Letters A*, *316*, 196–205.

Balthazar, J. M., Mook, D. T., Weber, H. I., Brasil, R. M. I. R. F., Fenili, A., Beltano, D., et al. (2003). An overview on non-ideal vibrations. *Meccanica*, *38*, 613–621.

Balthazar, J. L., & Brasil, R. M. L. R. F. (2004). On saturation control of a non-ideal vibrating portal frame founded type shear - building. *Journal of Vibration and Control*, *10*, 1739–1748.

Bogolyubov, N. N., & Mitropolskij, Ju. A. (1974). *Asimptoticheskie metodi v teorii nelinejnih kolebanij*. Moscow: Nauka.

Cveticanin, L. (2010). Dynamics of the non-ideal mechanical systems: A review. *Journal of the Serbian Society for Computational Mechanics*, *4*(2), 75–86.

Cveticanin, L. (2015). *Dynamics of bodies with time-variable mass*. Berlin: Springer. ISBN 978-3-319-22055-0.

Dantas, M. J. H., & Balthazar, J. M. (2007). On the existence and stability of periodic orbits in non ideal problems: General results. *Zeitschrift fur angewandteMathematik und Physik*, *58*, 940–958.

Dimentberg, M. F., McGovern, L., Norton, R. L., Chapdelaine, J., & Harrison, R. (1997). Dynamics of an unbalanced shaft interacting with a limited power supply. *Nonlinear Dynamics*, *13*, 171–187.

Felix, J. L., Balthazar, J. M., & Brasil, R. M. L. R. F. (2009). Comments on nonlinear dynamics of a non-ideal Duffing-Rayleigh oscillator: Numerical and analytical approaches. *Journal of Sound and Vibration*, *319*, 1136–1149.

Felix, J. L. P., Balthazar, J. M., & Dantas, M. J. H. (2011). On a nonideal (MRD) damper-electro-mechanical absorber dynamics. *International Journal of Bifurcation and Chaos*, *21*(10), 2871–2882.

Goncalves, P. J. P., Silveira, M., Pontes Junior, B. R., & Balthazar, J. M. (2014). The dynamic behavior of a cantilever beam coupled to a non-ideal unbalanced motor through numerical and experimental analysis. *Journal of Sound and Vibration*, *333*, 5115–5129.

Kononenko, V. O. (1969). *Vibrating systems with a limited power supply*. London: Iliffe Books Ltd.

Kononenko, V. O. (1980). *Nelinejnie kolebanija mehanicheskih system. Izabranie trudi*. Kiev: Naukova dumka.

Kovriguine, D. A. (2012). Synchronization and sommerfeld effect as typical resonant patterns. *Archive of Applied Mechanics*, *82*(5), 591–604.

Lin, R. M., & Ewins, D. J. (1993). Chaotic vibration of mechanical systems with backlash. *Mechanical Systems and Signal Processing*, *7*, 257–272.

Nayfeh, A. H., & Mook, D. T. (1976). *Nonlinear oscillations*. New York: Wiley.

Nayfeh, A. H., & Mook, D. T. (1979). *Nonlinear oscillations*. New York: Wiley-Interscience.

Ott, E., Grebogi, C., & Yorke, Y. A. (1990). Controlling chaos. *Physical Review Letter*, *64*, 1196–1999.

Pyragas, K. (1992). Continuous control of chaos by self controlling feedback. *Physics Letters A*, *170*, 421–428.

Pyragas, K. (1996). Continuous control of chaos by self-controlling feedback. *Controlling chaos* (pp. 118–123). San Diego: Academic Press.

Samantaray, A. K., Dasgupta, S. S., & Bhattacharyya, R. (2010). Sommerfeld effect in rotationally symmetric planar dynamical systems. *International Journal of Engineering Science*, *48*, 21–36.

Sandri, M. (1996). Numerical calculation of Lyapunov exponents. *The Mathematica Journal*, *6*, 78–84.

Souza, S. L. T., Caldas, I. L., Viana, R. L., Balthazar, J. M., & Brasil, R. M. L. R. F. (2005a). Impact dampers for controlling chaos in systems with limited power supply. *Journal of Sound and Vibration*, *279*, 955–965.

Souza, S. L. T., Caldas, I. L., Viana, R. L., Balthazar, J. M., & Brasil, R. M. L. R. F. (2005b). Basins of attraction changes by amplitude constraining of oscillators with limited power supply. *Chaos, Solitons and Fractals*, *26*, 1211–1220.

Tereshko, V., Chacon, R., & Preciado, V. (2004). Controlling chaotic oscillators by altering their energy. *Physics Letters A*, *320*, 408–416.

Tusset, A. M., Balthazar, J. M., Basinello, D. G., Pntes, B. R., & Felix, J. L. P. (2012a). Statements on chaos control designs, including fractional order dynamical system, applied to a „MEMS" conb-drive actuator. *Nonlinear Dynamics*, *69*(4), 1837–1857.

Tusset, A. M., Balthazar, J. M., Chavarette, F. R. & Felix, J. L. P. (2012b). On energy transfer phenpmena, in a nonlinear ideal and nonideal essential vibrating systems, coupled to a (MR) magneto-rheological damper. *Nonlinear Dynamics*, *69*(4), 1859–1880.

Warminski, J., Balthazar, J. M., & Brasil, R. M. L. R. F. (2001). Vibrations of a non-ideal parametrically and self-excited model. *Journal of Sound and Vibration*, *245*, 363–374.

Wolf, A. (1984). In Holden, A. V. (Ed.), *Quantifying chaos with Lyapunov exponent. Nonlinear science: Theory and application*. Manchester: Manchester University Press.

Wolf, A., Swift, J., Swinney, H., & Vastano, J. (1985). Determining Lyapunov exponents from a time series. *Physica D*, *16*, 285–317.

Zukovic, M., & Cveticanin, L. (2009). Chaos in non-ideal mechanical system with clearance. *Journal of Vibration and Control*, *15*, 1229–1246.